RESEARCH ARTICLE | SEPTEMBER 23 2013

Unsteady peristaltic transport in curved channels

J. V. Ramanamurthy; K. M. Prasad; V. K. Narla

Physics of Fluids 25, 091903 (2013)
https://doi.org/10.1063/1.4821355

PHYSICS OF FLUIDS **25**, 091903 (2013)

Unsteady peristaltic transport in curved channels

J. V. Ramanamurthy,[1] K. M. Prasad,[2] and V. K. Narla[2]
[1]*Department of Mathematics, National Institute of Technology, Warangal, Andhra Pradesh, India*
[2]*Department of Mathematics, GITAM University, Hyderabad, Andhra Pradesh, India*

(Received 18 April 2013; accepted 30 August 2013; published online 23 September 2013)

The paper presents a generalized mathematical model describing the unsteady peristaltic flow of a viscous fluid in a two-dimensional curved channel. The flow is investigated in a laboratory frame of reference and the unsteady flow nature is studied by the condition that prescribing volumetric flow rate is equivalent to prescribing normal velocity of the fluid particles at the wall. The momentum and energy equations have been linearized by employing lubrication theory and the analysis is restricted to negligible flow Reynolds number. The expressions for stream function, pressure distribution, shear stress, temperature, and coefficient of heat transfer have been derived. The obtained expressions are utilized to discuss the influences of various emerging parameters on flow phenomenon. © *2013 AIP Publishing LLC*. [http://dx.doi.org/10.1063/1.4821355]

I. INTRODUCTION

Peristalsis is a mechanism of fluid transport induced by a progressive wave of contraction or expansion propagating along the length of a flexible tube. It appears in the gastrointestinal tract, urine transport from kidney to bladder, bile from the gall bladder into the duodenum, the movement of spermatozoa in the ducts efferentes of the male reproductive tract, transport of lymph in the lymphatic vessels, and in the vasomotion of small blood vessels such as arterioles, venules, and capillaries. This process has quite useful applications in many biological systems and industry where it is found necessary to avoid contact between the pumped medium and the mechanical parts of the pump, for example, the blood pump in heart-lung machine and pumping of noxious fluid in nuclear industry.

The mathematical modeling of peristaltic transport has begun with the important works by Fung and Yih[1] using laboratory frame of reference and Shapiro *et al.*[2] using wave frame of reference. Many of the contributors to the area of peristaltic pumping have either followed Shapiro *et al.*[2] or Fung and Yih.[1] In the last two decades many investigations on peristaltic flow have been carried out by different authors for analytic and numerical studies.[1–10] Li and Brasseur[7] derived expressions of the non-steady pressure distribution and local wall shear stress for the axisymmetric case of a finite length tube. Dodds *et al.*[11] and Pal and Brasseur[12] investigated local longitudinal shortening of esophageal wall and its mechanical advantage on peristaltic transport. All these studies have been carried out in straight channel or tubes. In fact, the shape of most physiological ducts is curved in nature. The corresponding study of the peristaltic flow in curved channel was carried out by Sato *et al.*[13] Ali *et al.*[14] discussed the peristaltic motion in a curved channel using wave frame. Later, Ali *et al.*[15] extended the flow analysis by considering heat transfer effects. Non-Newtonian fluid flow induced by peristaltic waves in a curved channel has been investigated by Ali *et al.*[16] Hayat *et al.*[17] have examined the peristaltic flow of viscous fluid in a curved channel with complaint walls. Hayat *et al.*[18] have extended to investigate the effect of an induced magnetic field on the peristaltic flow of non-Newtonian fluid in a curved channel. Hina *et al.*[19–21] have examined wall properties of curved channels driven by peristalsis for different types of fluids. All these studies in curved channels of peristaltic transport of Newtonian and/or non-Newtonian fluids have analyzed the problem by neglecting the local dynamics such as spatial-temporal variations in the local pressure and stress.

Many problems related to physiological flows are solved by employing lubrication theory. This theory can be usefully applied when the gap between cell and vessel wall is small compared to the vessel radius and axial length. Some examples are the flows of synovial fluid within joints in the musculoskeletal system, physiological filtration of blood in the kidneys, fluid flows in ureter, and fallopian tubes.[22] The objective of this paper is to analyze the time dependent peristaltic transport in a finite length curved channel. In order to study the time-dependent fluid pattern, lubrication theory has been employed. Hence, the analysis in the present model is carried out, assuming zero Reynolds number and that the ratio of the channel radius to the wavelength of the peristaltic wave is invariably small. Further, the unsteady effects are observed under the condition that prescribing flow rate is equivalent to prescribing normal velocity of the fluid at the wall. The expressions for the stream function, temperature, pressure distribution, shear stress, and heat transfer coefficient are calculated. The influences of various emerging parameters on peristalsis over time are discussed by plotting graphs.

II. MATHEMATICAL MODEL

A. Governing equations

We consider a two-dimensional flow of an incompressible viscous fluid in a curved channel of unperturbed width $2a$. The channel is coiled in a circle with center O and radius R. We choose a curvilinear coordinate system (x, r) in such a way that the x-axis lies along the centerline of the curved channel and the r-axis is normal to it and is measured from central line with scaling factors $h_1 = \frac{r+R}{R}$, $h_2 = 1$, and $h_3 = 1$. There is no component in the z direction as shown in Figure 1. The fluid flow in the curved channel gives velocity vector in the form $\overline{V} = u(x, r, t)\widehat{e}_x + v(x, r, t)\widehat{e}_r$. The fluid motion within the channel is induced by two infinite trains of sinusoidal waves that are propagated along the flexible channel walls described as

$$r = h(x, t) = a + bcos\left[2\pi\left(\frac{x}{\lambda} - \frac{t}{T^*}\right)\right] \text{ (Upper wall)}, \tag{1}$$

$$r = -h(x, t) = -a - bcos\left[2\pi\left(\frac{x}{\lambda} - \frac{t}{T^*}\right)\right] \text{ (Lower wall)}. \tag{2}$$

In the above equations, a is the radius of the stationary curved channel, b is the wave amplitude, λ is the wavelength, t is the time, T^* is the wave period, and h is the radial displacement of the wave from the centerline. The temperatures of the lower and upper walls are maintained at constant temperatures T_0 and T_1, respectively.

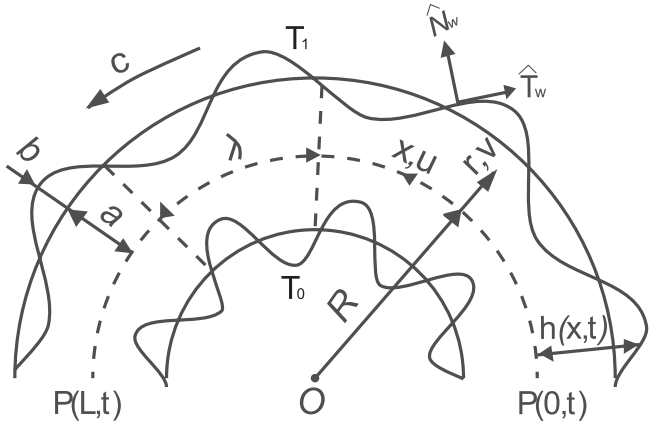

FIG. 1. Peristaltic wave in a curved channel.

The conservation equations (mass and momentum) for the curved channel in the absence of body force can be written as (Sato *et al.*[13])

$$R\frac{\partial u}{\partial x}+\frac{\partial}{\partial r}\{(r+R)v\}=0, \tag{3}$$

$$\frac{\partial u}{\partial t}+(\overline{V}\cdot\nabla)u+\frac{uv}{r+R}=-\frac{R}{\rho(r+R)}\frac{\partial p}{\partial x}+\nu\Big[\nabla^2u-\frac{u}{(r+R)^2}+\frac{2R}{(r+R)^2}\frac{\partial v}{\partial x}\Big], \tag{4}$$

$$\frac{\partial v}{\partial t}+(\overline{V}\cdot\nabla)v-\frac{u^2}{r+R}=-\frac{1}{\rho}\frac{\partial p}{\partial r}+\nu\Big[\nabla^2v-\frac{v}{(r+R)^2}-\frac{2R}{(r+R)^2}\frac{\partial u}{\partial x}\Big], \tag{5}$$

$$C_p\Big[\frac{\partial T}{\partial t}+(\overline{V}\cdot\nabla)T\Big]=\frac{K}{\rho}\nabla^2T+\nu\Big[2\Big\{\Big(\frac{\partial v}{\partial r}\Big)^2+\Big(\frac{R}{r+R}\frac{\partial u}{\partial x}+\frac{v}{r+R}\Big)^2\Big\}+\Big(\frac{\partial u}{\partial r}+\frac{R}{r+R}\frac{\partial v}{\partial x}-\frac{u}{r+R}\Big)^2\Big], \tag{6}$$

where

$$(\overline{V}\cdot\nabla)=\frac{Ru}{(r+R)}\frac{\partial}{\partial x}+v\frac{\partial}{\partial r}, \tag{7}$$

$$\nabla^2=\Big(\frac{R}{r+R}\Big)^2\frac{\partial^2}{\partial x^2}+\frac{1}{r+R}\frac{\partial}{\partial r}+\frac{\partial^2}{\partial r^2}. \tag{8}$$

Here, p, ν, ρ, t, C_p, K, and T are the pressure, kinematic viscosity, fluid density, time, specific heat, thermal conductivity, and temperature, respectively.

The fluid velocity satisfies the following conditions at the wall ($r=\pm h(x,t)$):

1. The tangential fluid velocity is zero at the wall:

$$\overline{V}\cdot\widehat{T}_W=0. \tag{9}$$

2. The normal velocity of fluid at the wall is given by

$$\overline{V}\cdot\widehat{N}_W=V_W, \tag{10}$$

where $\widehat{T}_W$ and $\widehat{N}_W$ are the unit tangent and normal vectors at the wall, respectively,

$$\widehat{T}_W=\frac{\widehat{e}_x+\frac{\partial h}{\partial x}\widehat{e}_r}{\sqrt{1+(\frac{\partial h}{\partial x})^2}} \tag{11}$$

and

$$\widehat{N}_W=\frac{-\frac{\partial h}{\partial x}\widehat{e}_x+\widehat{e}_r}{\sqrt{1+(\frac{\partial h}{\partial x})^2}}. \tag{12}$$

The definition of the stream function ψ, which satisfies continuity equation, can be written as

$$u=\frac{\partial\psi}{\partial r},\ v=-\frac{R}{r+R}\frac{\partial\psi}{\partial x}. \tag{13}$$

B. Lubrication theory

The governing equations can be linearized by employing lubrication approximation. In the present model there are three characteristic lengths a, b, and λ. It is assumed that the wavelength is large compared with the channel's width $\lambda\gg a$. In addition, we do not restrict the magnitude of the wave amplitude b, except that it cannot exceed the channel radius that is $b\ll a$, which yields that

the local slope of the channel wall is small. Under these assumptions, the model then has certain similarities in scaling to the lubrication theory analysis.[22] In order to describe the fluid flow pattern in dimensionless form, the variables are scaled as follows:

$$x' = \frac{x}{\lambda}, r' = \frac{r}{a}, u' = \frac{u}{c}, v' = \frac{v}{\delta c}, h' = \frac{h}{a}, \phi = \frac{b}{a}, \kappa = \frac{R}{a}, t' = \frac{t}{T^*}, L' = \frac{L}{\lambda},$$
$$p' = \frac{a^2 p}{\mu c \lambda}, Re = \frac{ca\delta}{\nu}, \psi' = \frac{\psi}{ac}, F = \frac{Q}{ac}, P_r = \frac{\rho \nu C_p}{K}, E = \frac{c^2}{C_p(T_1 - T_0)}, \theta = \frac{T - T_0}{T_1 - T_0}, \tag{14}$$

in which Re is the Reynolds number, F is the volume flow rate, $c = \frac{\lambda}{T^*}$ is the velocity of the wave, $\delta = \frac{a}{\lambda}$ is the wave number, ϕ is the amplitude ratio or the occlusion parameter, κ is the curvature parameter, L is the length of the channel, P_r is the Prandtl number, and E is the Eckert number. The non-dimensional form of Eqs. (3)–(6) with the help of Eq. (14) after dropping the primes takes the form

$$\frac{\kappa}{r+\kappa}\frac{\partial u}{\partial x} + \frac{\partial v}{\partial r} + \frac{v}{r+\kappa} = 0, \tag{15}$$

$$Re\delta\left[\frac{\partial u}{\partial t} + (\overline{V}\cdot\nabla)u + \frac{uv}{r+\kappa}\right] = -\frac{\kappa}{(r+\kappa)}\frac{\partial p}{\partial x} + \nabla^2 u - \frac{u}{(r+\kappa)^2} + \delta^2\frac{2\kappa}{(r+\kappa)^2}\frac{\partial v}{\partial x}, \tag{16}$$

$$Re\delta\left[\delta^2\left(\frac{\partial v}{\partial t} + (\overline{V}\cdot\nabla)v\right) - \frac{u^2}{r+\kappa}\right] = -\frac{\partial p}{\partial r} + \delta^2\left[\nabla^2 v - \frac{v}{(r+\kappa)^2} - \frac{2\kappa}{(r+\kappa)^2}\frac{\partial u}{\partial x}\right], \tag{17}$$

$$P_r Re\delta\left[\frac{\partial \theta}{\partial t} + (\overline{V}\cdot\nabla)\theta\right] = \nabla^2\theta + Br\left[2\delta^2\left\{\left(\frac{\partial v}{\partial r}\right)^2 + \left(\frac{\kappa}{r+\kappa}\frac{\partial u}{\partial x} + \frac{v}{r+\kappa}\right)^2\right\} + \left(\frac{\partial u}{\partial r} + \delta^2\frac{\kappa}{r+\kappa}\frac{\partial v}{\partial x} - \frac{u}{r+\kappa}\right)^2\right], \tag{18}$$

where

$$(\overline{V}\cdot\nabla) = \frac{\kappa u}{(r+\kappa)}\frac{\partial}{\partial x} + v\frac{\partial}{\partial r}, \tag{19}$$

$$\nabla^2 = \delta^2\left(\frac{\kappa}{r+\kappa}\right)^2\frac{\partial^2}{\partial x^2} + \frac{1}{r+\kappa}\frac{\partial}{\partial r} + \frac{\partial^2}{\partial r^2}, \tag{20}$$

where $Br = PrE$ is the Brinkman number. In view of Eqs. (9) and (10), the boundary conditions can be represented as

$$u + \delta^2\frac{\partial h}{\partial x}v = 0, \qquad at\ r = \pm h, \tag{21}$$

$$v - \frac{\partial h}{\partial x}u = V_W\left[\left\{1 + \delta^2\left(\frac{\partial h}{\partial x}\right)^2\right\}^{\frac{1}{2}}\right], \qquad at\ r = \pm h, \tag{22}$$

$$\theta = 0, \qquad at\ r = -h(x,t), \tag{23}$$

and

$$\theta = 1, \qquad at\ r = h(x,t). \tag{24}$$

C. Rate of volume flux and boundary conditions

The dimensional volume flow rate in laboratory frame is defined as

$$Q(x,t) = \int_{-h}^{h} u(x,r,t)dr. \tag{25}$$

The flow rate (25) in wave frame is defined as

$$Q(x,t) = q(x) + 2ch(x,t), \tag{26}$$

and the time averaged flow rate over a period T, yielding

$$Q_T(x) = \frac{1}{T}\int_0^T Q(x,t)dt = q(x) + 2ac. \tag{27}$$

It may be noted that for incompressible flow, prescribing volume flow rate is equivalent to prescribing normal velocity (V_W) of the fluid at the wall. This is related via mass conservation equation (3),

$$\frac{\partial Q}{\partial x}(x,t) + \frac{\partial A}{\partial t}(x,t) = 0, \tag{28}$$

where $A(x, t)$ is the cross sectional area. Integrating (28) with respect to x, we get

$$Q(x,t) = Q(0,t) - \int_0^x \frac{\partial A}{\partial t}(x,t)dx, \tag{29}$$

where $Q(0, t)$ is the flow rate at $x = 0$. However, due to equation of continuity (3), $Q_T(x) = Q_T$, for every x. Then the non-dimensional form of volumetric flux can be obtained by substituting $q(x)$ from (27) into (26) and scaled with ac as

$$F(x,t) = Q_T + 2(h(x,t) - 1). \tag{30}$$

The stream function ψ in Eq. (13) in dimensionless form can be defined as

$$u = \frac{\partial \psi}{\partial r}, \quad v = -\frac{\kappa}{r+\kappa}\frac{\partial \psi}{\partial x}, \tag{31}$$

$$F(x,t) = \int_{-h}^{h} \frac{\partial \psi}{\partial r}dr = \psi(h) - \psi(-h). \tag{32}$$

By the choice of $\psi(h) = \frac{F}{2}$ and $\psi(-h) = -\frac{F}{2}$, Eqs. (16)–(18) can be written under the assumptions of lubrication theory and low Reynolds number flow approximation as

$$\nabla^4 \psi = 0, \tag{33}$$

$$\frac{\partial^2 \theta}{\partial r^2} + \frac{1}{r+\kappa}\frac{\partial \theta}{\partial r} + Br\left(\frac{\partial u}{\partial r} - \frac{u}{r+\kappa}\right)^2 = 0, \tag{34}$$

where

$$\nabla^2 = \frac{1}{r+\kappa}\frac{\partial}{\partial r}\left\{(r+\kappa)\frac{\partial}{\partial r}\right\}.$$

The dimensionless boundary conditions can be obtained by using Eqs. (21)–(24), and (29) as follows:

$$\frac{\partial \psi}{\partial r} = 0, \text{ at } r = \pm h(x,t), \tag{35}$$

$$\psi = \frac{1}{2}\left[F(0,t) - 2\int_0^x \frac{\partial h}{\partial t}(s,t)ds\right], \text{ at } r = h(x,t), \tag{36}$$

$$\psi = -\frac{1}{2}\Big[F(0,t) - 2\int_0^x \frac{\partial h}{\partial t}(s,t)ds\Big], \text{ at } r = -h(x,t), \tag{37}$$

$$\theta = 0, \text{ at } r = -h(x,t) \text{ and } \theta = 1, \text{ at } r = h(x,t), \tag{38}$$

where $F(0, t)$ is the volume flow rate at channel inlet.

III. SOLUTION OF THE PROBLEM

The solutions of Eqs. (33) and (34) with the boundary conditions Eqs. (35)–(38) are in the form

$$\psi = C_1(x,t) + C_2(x,t)log(r+\kappa) + C_3(x,t)(r+\kappa)^2 + C_4(x,t)(r+\kappa)^2 log(r+\kappa),$$

$$C_1(x,t) = \frac{F\left[2h\kappa(h^2+\kappa^2) + \left\{(log\frac{\kappa+h}{\kappa-h}) + (log(\kappa-h))^2 - (log(\kappa+h))^2\right\}(h^2-\kappa^2)^2\right]}{2\left[-4h^2\kappa^2 + (h^2-\kappa^2)^2(log\frac{\kappa-h}{\kappa+h})^2\right]},$$

$$C_2(x,t) = -\frac{F(h^2-\kappa^2)^2 log\frac{\kappa-h}{\kappa+h}}{-4h^2\kappa^2 + (h^2-\kappa^2)^2(log\frac{\kappa-h}{\kappa+h})^2}, \tag{39}$$

$$C_3(x,t) = \frac{F[-2h\kappa + (h-\kappa)^2 log(\kappa-h) - (h+\kappa)^2 log(h+\kappa)]}{2[-4h^2\kappa^2 + (h^2-\kappa^2)^2(log\frac{\kappa-h}{\kappa+h})^2]},$$

$$C_4(x,t) = \frac{2Fh\kappa}{-4h^2\kappa^2 + (h^2-\kappa^2)^2(log\frac{\kappa-h}{\kappa+h})^2},$$

and

$$\theta = A_1(x,t) + A_2(x,t)log(r+\kappa) - Br\left[C_4^2(r+\kappa)^2 + C_2^2(r+\kappa)^{-2} - 4C_2C_4(log(r+\kappa))^2\right],$$

$$A_1(x,t) = \frac{1}{log\frac{\kappa-h}{\kappa+h}}\Big[Br\Big\{C_2^2\Big(\frac{log(\kappa-h)}{(\kappa+h)^2} - \frac{log(\kappa+h)}{(\kappa-h)^2}\Big) + C_4^2((\kappa+h)^2 log(\kappa-h) - (\kappa-h)^2 log(\kappa+h))$$

$$-4C_2C_4\Big((log(\kappa+h))^2 log(\kappa-h) - (log(\kappa-h))^2 log(\kappa+h)\Big)\Big\} + log(\kappa-h)\Big], \tag{40}$$

$$A_2(x,t) = \frac{1}{log\frac{\kappa+h}{\kappa-h}}\left[1 - 4Br\left\{\frac{C_2^2 h\kappa}{(\kappa-h)^2(\kappa+h)^2} - C_4^2 h\kappa + C_2C_4\Big((log(\kappa+h))^2 - (log(\kappa-h))^2\Big)\right\}\right].$$

Moreover, the expression of the axial pressure gradient can be obtained from Eqs. (16), (31), and (39) as

$$\frac{\partial p}{\partial x} = \frac{H(t) + 16\int_0^x \frac{\partial h(s,t)}{\partial t}ds}{4\kappa^2 h(x,t) - \frac{(h^2(x,t)-\kappa^2)^2}{h(x,t)}\Big(log(\frac{\kappa-h(x,t)}{\kappa+h(x,t)})\Big)^2}, \tag{41}$$

where $H(t) = -8F(0, t)$. Integrating Eq. (41) between 0 and x yields the intraluminal pressure distribution function in the form

$$\Delta P = p(x,t) - p(0,t) = \int_0^x \frac{H(t) + 16\int_0^s \Big(\frac{\partial h(u,t)}{\partial t}\Big)du}{4\kappa^2 h(s,t) - \frac{(h^2(s,t)-\kappa^2)^2}{h(s,t)}\Big(log\Big(\frac{\kappa-h(s,t)}{\kappa+h(s,t)}\Big)\Big)^2}ds. \tag{42}$$

The integrating constant function $H(t)$ is determined by evaluating (42) at $x = L$ and is given by

$$H(t) = \frac{\Delta P_L(t) - \int_0^L \frac{16 \int_0^x \frac{\partial h(s,t)}{\partial t} ds}{4\kappa^2 h(x,t) - \frac{(h^2(x,t)-\kappa^2)^2}{h(x,t)} \left[log\left(\frac{\kappa - h(x,t)}{\kappa + h(x,t)}\right)\right]^2} dx}{\int_0^L \frac{1}{4\kappa^2 h(x,t) - \frac{(h^2(x,t)-\kappa^2)^2}{h(x,t)} \left[log\left(\frac{\kappa - h(x,t)}{\kappa + h(x,t)}\right)\right]^2} dx}. \tag{43}$$

Here, $\Delta P_L(t) = p(L, t) - p(0, t)$ is the pressure difference across the channel ends.

From Eq. (27), the axial pressure gradient in terms of time-averaged flow can be presented in the form

$$\frac{\partial p(x,t)}{\partial x} = \frac{-8(Q_T(x) + 2(h-1))}{\left[4\kappa^2 h - \frac{(\kappa^2 - h^2)^2}{h} \left(log \frac{\kappa + h}{\kappa - h}\right)^2\right]}. \tag{44}$$

The local wall shear stress derived at the upper and lower walls is, respectively,

$$\tau_{Upper}(x,t) = \frac{\partial p(x,t)}{\partial x} \left[\frac{2\kappa h(x,t) + (h(x,t) - \kappa)^2 log\left(\frac{\kappa - h(x,t)}{\kappa + h(x,t)}\right)}{4h(x,t)} \right] \tag{45}$$

and

$$\tau_{Lower}(x,t) = \frac{\partial p(x,t)}{\partial x} \left[\frac{2\kappa h(x,t) + (h(x,t) + \kappa)^2 log\left(\frac{\kappa - h(x,t)}{\kappa + h(x,t)}\right)}{4h(x,t)} \right]. \tag{46}$$

The heat transfer coefficient at the upper and lower walls is denoted by

$$Z = \frac{\partial h}{\partial x} \cdot \frac{\partial \theta}{\partial r}\Big|_{r=\pm h}. \tag{47}$$

The heat transfer coefficient at the upper wall is

$$Z_{Upper} = \frac{\partial h}{\partial x} \left[\frac{A_2}{h + \kappa} - Br \left\{ 2c_4^2 (h + \kappa) - 2c_2^2 (h + \kappa)^{-3} - 8c_2 c_4 \frac{log(h + \kappa)}{h + \kappa} \right\} \right]. \tag{48}$$

The heat transfer coefficient at the lower wall is

$$Z_{Lower} = \frac{\partial h}{\partial x} \left[\frac{A_2}{-h + \kappa} - Br \left\{ 2c_4^2 (-h + \kappa) - 2c_2^2 (-h + \kappa)^{-3} - 8c_2 c_4 \frac{log(-h + \kappa)}{-h + \kappa} \right\} \right]. \tag{49}$$

IV. NUMERICAL RESULTS AND DISCUSSION

A. Local pressure distribution

The investigation of time dependent pressure distribution of the peristaltic flow along the axial distance of integral and non-integral multiple of wavelength is conducted for time instants t from 0 to 1. The following discussion pertains to the case of free pumping only ($\Delta P_L(t) = 0$). In such a case, the flow is due only to the traveling peristaltic waves when the pressures imposed at the two ends of the channel are equal. We consider two wave trains propagating along the walls of the channel. When the fluid enters the channel through its inlet, a bolus is created which moves with the wave. This is possible only when the local pressure gradient is negative. In the case of integral number of train wave propagation (say $L = 2$), Figure 2 is plotted between the pressure difference ΔP and the axial distance x at different time points for various curvature parameters ($\kappa = 1.5, 2, 5, \infty$). It is observed that the pressure is at its maximal peak near the tail of the bolus, and monotonically decreases to zero at the middle point of the bolus, and further it declines to a trough from where it finally rises sharply to meet the leading end of the bolus so as to transport it under huge control.

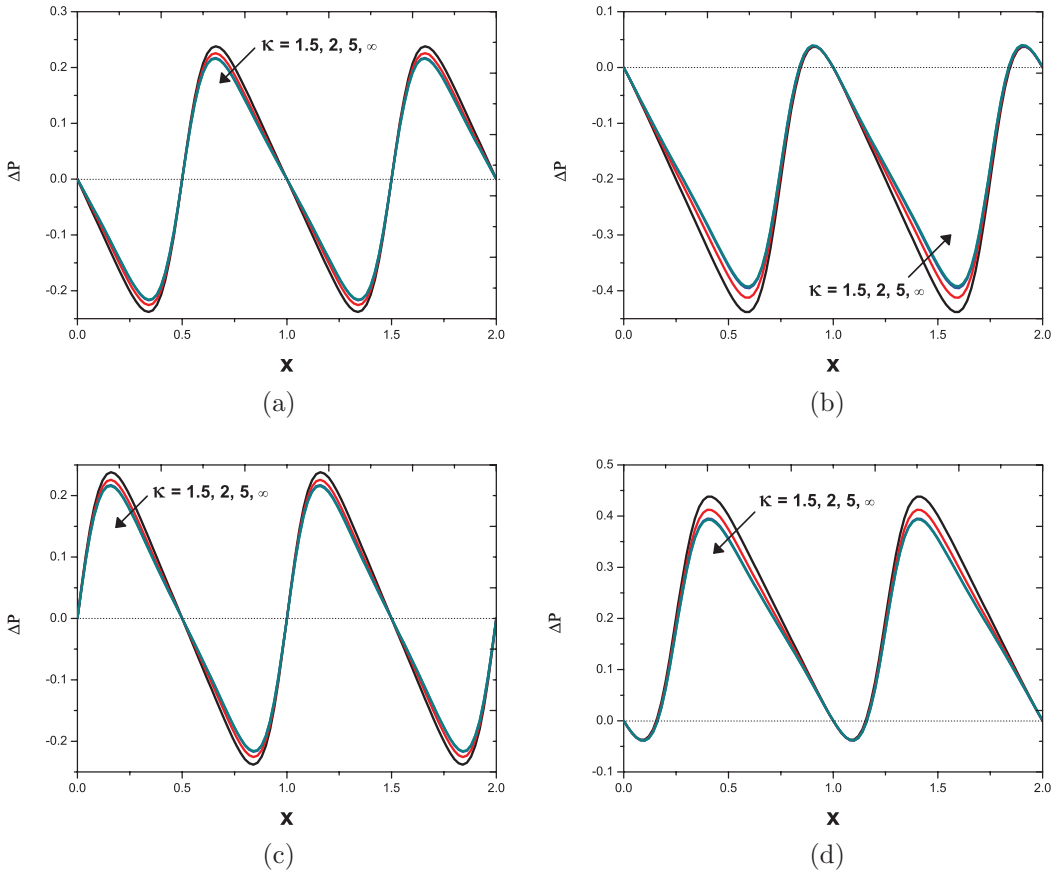

FIG. 2. Pressure distributions along the curved channel length at five time instants for different κ values when $\Delta P_L = 0$, $L = 2$, and $\phi = 0.4$, in case a train of two waves propagates along the channel. (a) $t = 0.0$ and 1.0; (b) $t = 0.25$; (c) $t = 0.5$; (d) $t = 0.75$.

It must be noted that the process gets repeated after each cycle. The following information can be observed from Figure 2.

- The increase in the curvature parameter κ causes a decrease in the magnitude of pressure difference ΔP. This means that the peristaltic flow pumping is lower in magnitude for straight channel than for curved channel. It may therefore be concluded that peristalsis has to work against greater pressure rise in curved channel as compared to flow in straight channel. In other words, it requires more pressure to propel the fluids in curved channel than in the straight channel.
- The pressure difference is not symmetric about the line where it changes its sign for the intermediate times t=0.25 and t=0.75. However, it is symmetric at t=0.0, t=0.5, and t=1.
- The magnitude of pressure difference (ΔP) is much higher in narrow parts of the curved channel for t=0.25 and 0.75 in comparison with the case for t=0.0, 0.5, and 1.
- The pressure distributions at time instants t=0.0 and t=1 are same. This indicates that the process is repeated periodically after each cycle due to periodic motion of the boundary.

The pressure distribution along the axis of non-integral multiple of wavelength is depicted in Figure 3. The significant difference between the two cases is that the peaks of the pressure for the two different types of boluses are not the same in magnitude in the non-integral case (i.e., the pressure difference attains two different maximum or minimum values over the whole length of the channel). For an integral case, the peak values of the pressure difference over the whole length of the channel are equal. This has been reported for straight channel by Li and Brasseur.[7]

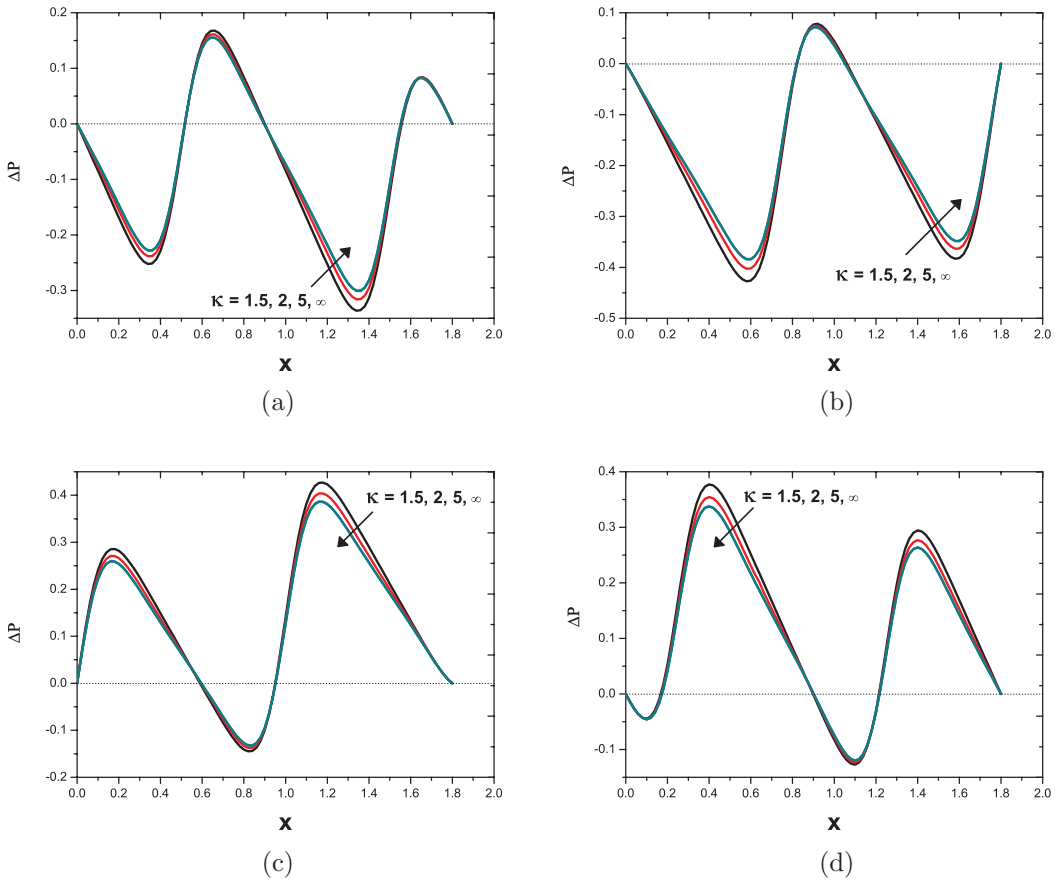

FIG. 3. Pressure distributions along the curved channel length at five time instants for different κ values when $\Delta P_L = 0$, $L = 1.8$, and $\phi = 0.4$, in case a train of two waves propagates along the channel. (a) $t = 0.0$ and 1.0; (b) $t = 0.25$; (c) $t = 0.5$; (d) $t = 0.75$.

The dependency of axial pressure difference on the length of the channel is depicted in Figure 4 for an adverse pressure $\Delta P_L > 0$ (opposing the flow direction) for integral and non-integral multiple of wavelengths. As ΔP_L increases, the pressure differences as well as maximal pressure values increase, and the minimal pressure value decreases in both the cases. The effects of occlusion parameter (amplitude ratio) ϕ on ΔP are shown in Figure 5. Pressure difference ΔP increases with increase of ϕ. The differences are observed for both the cases of integral and non-integral multiple of wavelengths. ΔP varies periodically for integral case and the variation in ΔP for the non-integral case is not periodic.

A relation between pressure difference over one wavelength ΔP_1 and time averaged flow rate Q_T is shown in Figure 6 for different values of curvature parameter κ. This figure reveals that the pressure difference ΔP_1 decreases as $\kappa \to \infty$ when the flow rate is below a critical value $Q_T < Q_{T_C}$ and if the flow rate is above this critical value Q_{T_C}, ΔP_1 increases as the channel curvature is decreased. An increase in the flow rate reduces the pressure difference; thus, maximum ΔP_1 is obtained at zero flow rate and vice versa. This means that in free pumping or co-pumping the flow rate is low and pressure difference is high for curved channel as compared to straight channel.

B. Shear stress distribution

The examination of shear stress in a flow field is a significant problem, because high shear stress may cause damage to blood elements, when blood is employed as the working fluid. The same reason holds in applications involving the transport of sensitive materials. In order to investigate the

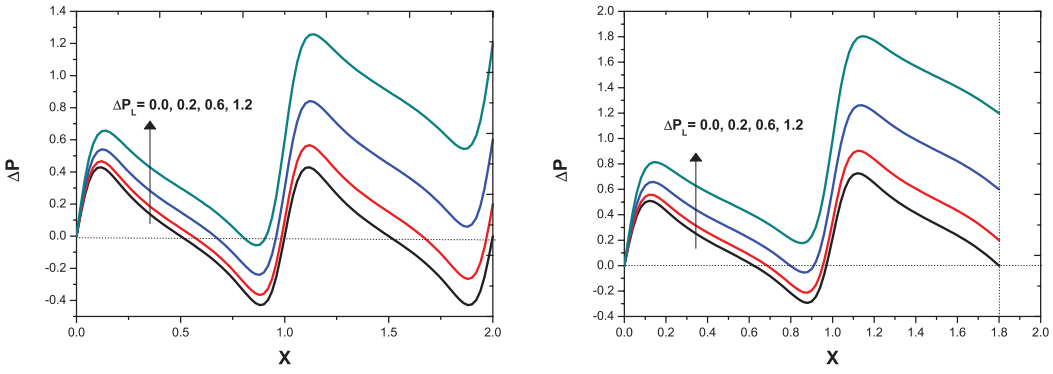

FIG. 4. The dependency of the axial pressure for pressure difference between channel ends when $\phi = 0.6$, $t = 0.5$, $\kappa = 2$ for (a) integral multiple of wavelength and (b) non-integral multiple of wavelength.

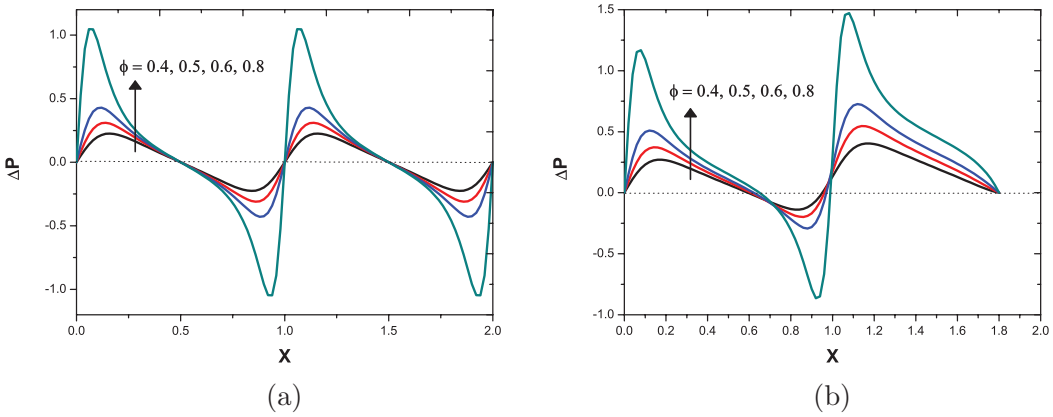

FIG. 5. The dependency of the axial pressure at different amplitude ratio $\phi = (\frac{b}{a})$ values when $\kappa = 2$, $\Delta P_L = 0.0$, $t = 0.5$ for (a) integral multiple of wavelength and (b) non-integral multiple of wavelength.

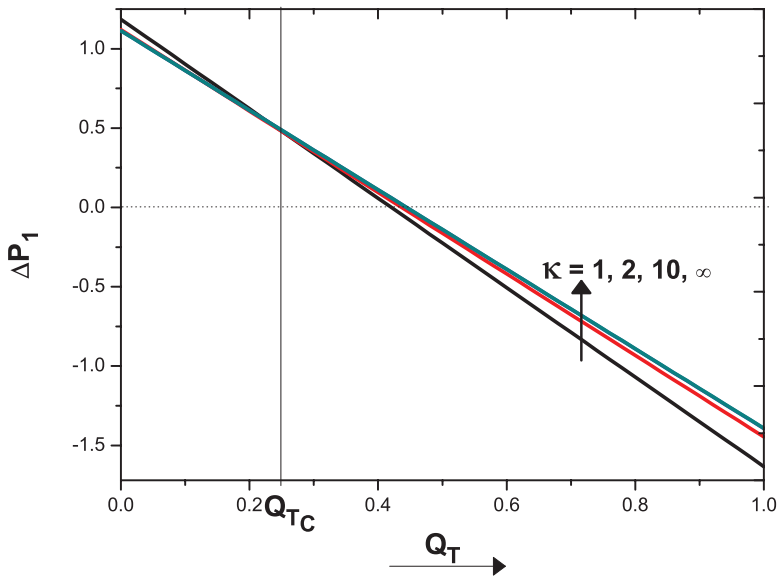

FIG. 6. Pressure difference across one wavelength against time-averaged flow rate for different values of curvature parameter κ with $\phi = 0.4$.

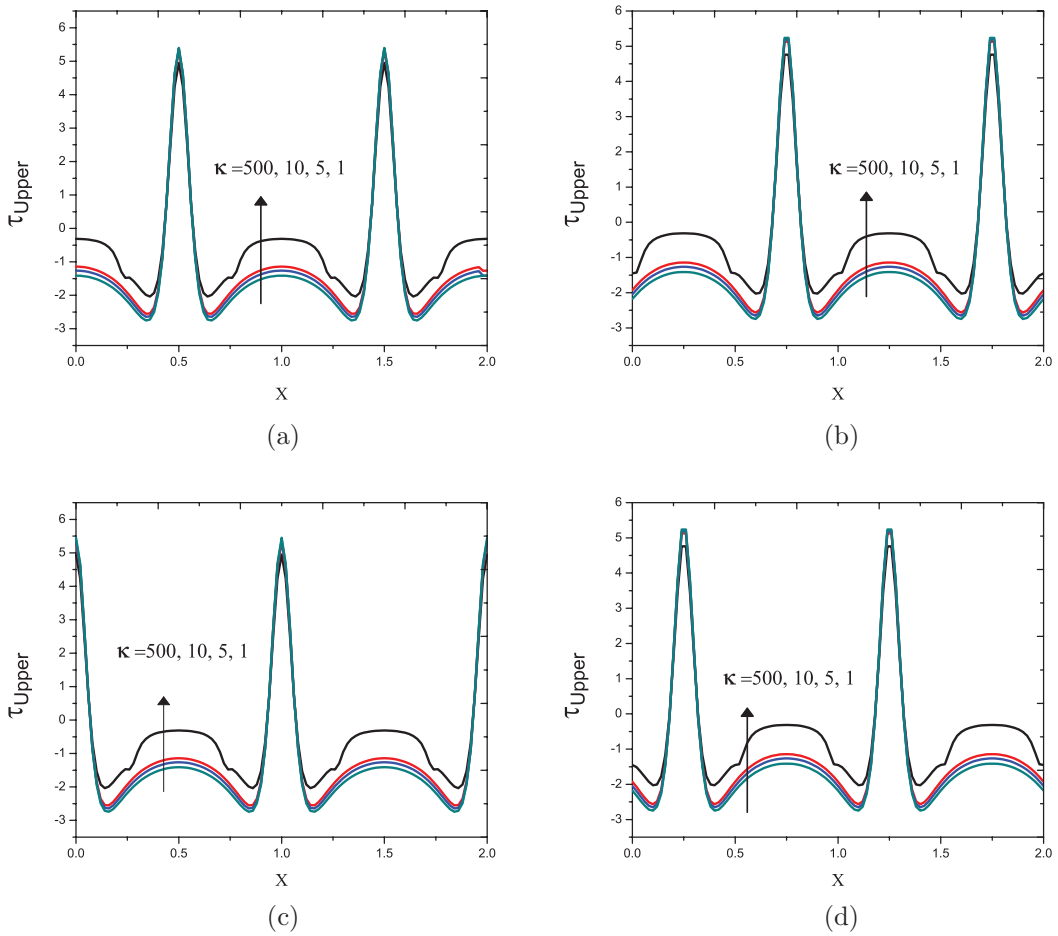

FIG. 7. Local shear stress at upper wall along the curved channel length at five time instants for different κ values when $\Delta P_L = 0, \phi = 0.4$, and $L = 2$. (a) $t = 0.0$ and 1.0; (b) $t = 0.25$; (c) $t = 0.5$; (d) $t = 0.75$.

magnitude of the shear stress for different curvature parameter values κ in the flow region, we plot shear stress τ at upper and lower walls for different times (Figures 7 and 8). As peristaltic wave moves in the axial direction, at time $t = 0.5$ (where two boluses appear completely) for upper wall, the shear stress declines eventually, reaches the lowest point from where it again rises until it reaches the middle of the wave. It must be noted that the shear stress distribution gets repeated after each cycle, and appears as the exact replica of the former cycle. It is further observed that at the leading edge of expansion segment of the peristaltic wave shear stress decreases and at the tailing edge it increases. The same is exactly opposite for contraction segment.

A significant quantitative difference is observed in the change of the shear stress at upper and lower walls. The negative peaks at lower wall are larger and deeper than the positive peaks at upper wall. It is further observed that the shear stress at the walls increases with an increasing channel curvature. This conveys that shear stress is more for curved channels and is less for straight channels.

C. Stream lines and trapping

The dimensional form of the stream function in the wave frame is defined as

$$d\psi = udr - vdx, \tag{50}$$

where ψ, x, r, u, and v are the stream function, the axial and transverse coordinates, and the axial and transverse velocities, respectively. The transformations between wave frame and laboratory frame

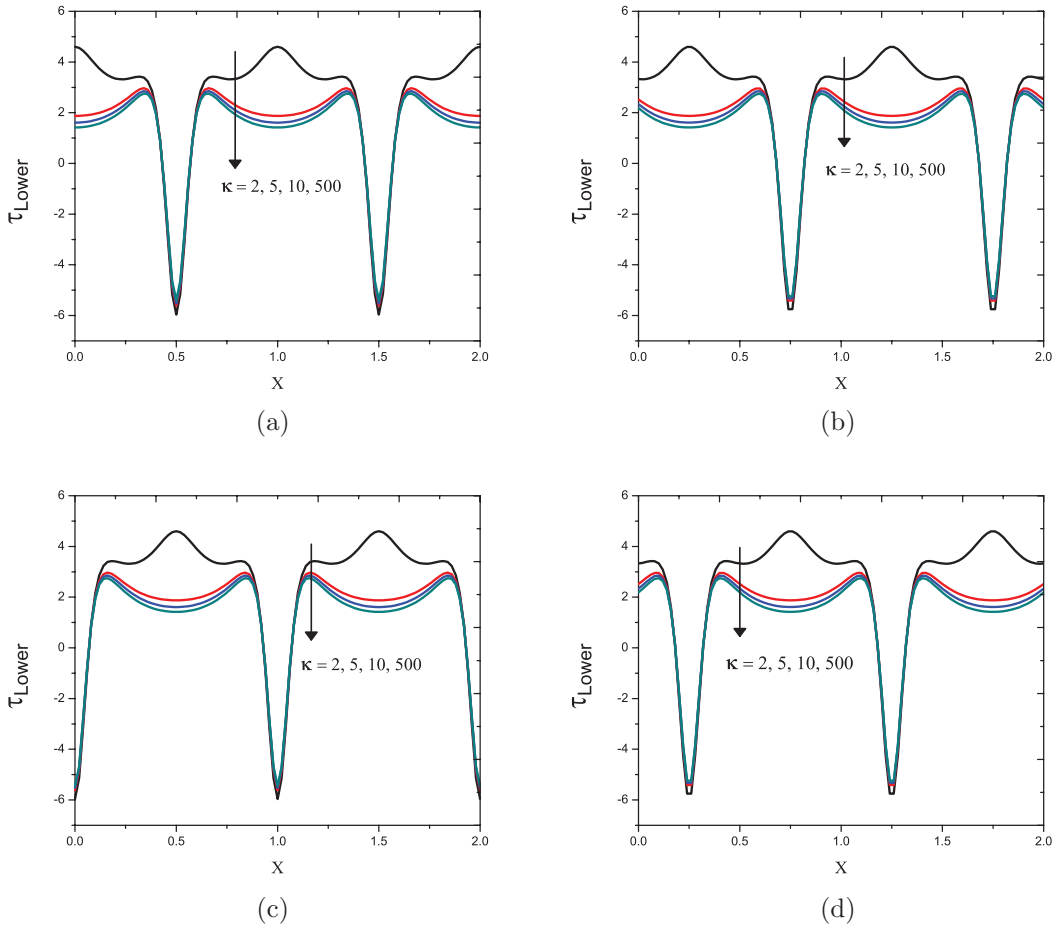

FIG. 8. Local shear stress at lower wall along the curved channel length at five time instants for different κ values when $\Delta P_L = 0, \phi = 0.4$, and $L = 2$. (a) $t = 0.0$ and 1.0; (b) $t = 0.25$; (c) $t = 0.5$; (d) $t = 0.75$.

are given by

$$X = x - ct, Y = r, U = u - c, V = v, q = Q - ch, \Psi = \psi - r, \tag{51}$$

where the parameters on the left side are in the wave frame and that on the right side are in the laboratory frame (fixed frame). In the wave frame the stream lines in general have a shape similar to the shape of the stationary walls. But under certain conditions some stream lines split (due to the existence of a stagnation point) to enclose a bolus of fluid particles which is called trapping. The fluid particles contained in the bolus advance at a mean speed exactly equal to the wave speed. The remaining fluid has a smaller mean speed than the wave speed. In the fixed frame the bolus moves as a whole with the wave speed as if it were trapped by the wave. This physical phenomena may be responsible for thrombus formation in blood and the movement of food bolus in gastrointestinal tract.

The criterion for central streamline trapping is the existence of stagnation points where both the velocity components u and v vanish in the wave frame and they are located at the intersections of the curve $\psi = 0$ and the centerline. From this analysis one can obtain the stagnation points given by the equation

$$\frac{\partial \Psi}{\partial r} \mid_{r=0} = \frac{(-2 + 2h + Q_T)hN_1}{-4h^2\kappa^3 + \kappa(h^2 - \kappa^2)^2(log\frac{\kappa+h}{\kappa-h})^2} = 1, \tag{52}$$

where

$$N_1 = 4\kappa^3 log\kappa - (h-\kappa)^2(h+2\kappa)log(\kappa-h) + (h+\kappa)^2(h-2\kappa)log(h+\kappa).$$

This implies

$$Q_T = 2 - 2h + \frac{4h^2\kappa^3 - \kappa(h^2-\kappa^2)^2(log\frac{\kappa+h}{\kappa-h})^2}{h\left[-4\kappa^3 log\kappa + (h-\kappa)^2(h+2\kappa)log(\kappa-h) - (h-2\kappa)(h+2\kappa)^2 log(\kappa+h)\right]}. \tag{53}$$

The stagnation points are real if the roots of Eq. (52) satisfy (Jaffrin[3])

$$1 - \phi \le h \le 1 + \phi.$$

One gets the central line trapping limits by analyzing Eq. (53)

$$Q_L \le Q_T \le Q_U,$$

where $Q_L = Q_T|_{h=1+\phi}$ and $Q_U = Q_T|_{h=1-\phi}$.

The streamlines patterns in the wave frame with $\phi = 0.4$ and $Q_T = 1.5$ for different values of curvature parameter κ are shown in Figure 9. It is important to observe that the trapped bolus of fluid comprises two asymmetrical boluses. The trapped bolus near the upper wall increases but the bolus at lower wall decreases and it disappears completely with an increasing channel curvature (small values of κ). That means for small values of κ only one bolus is formed near to upper wall that can be observed when $\kappa = 2$. One can observe further that the sizes of the trapped bolus in the

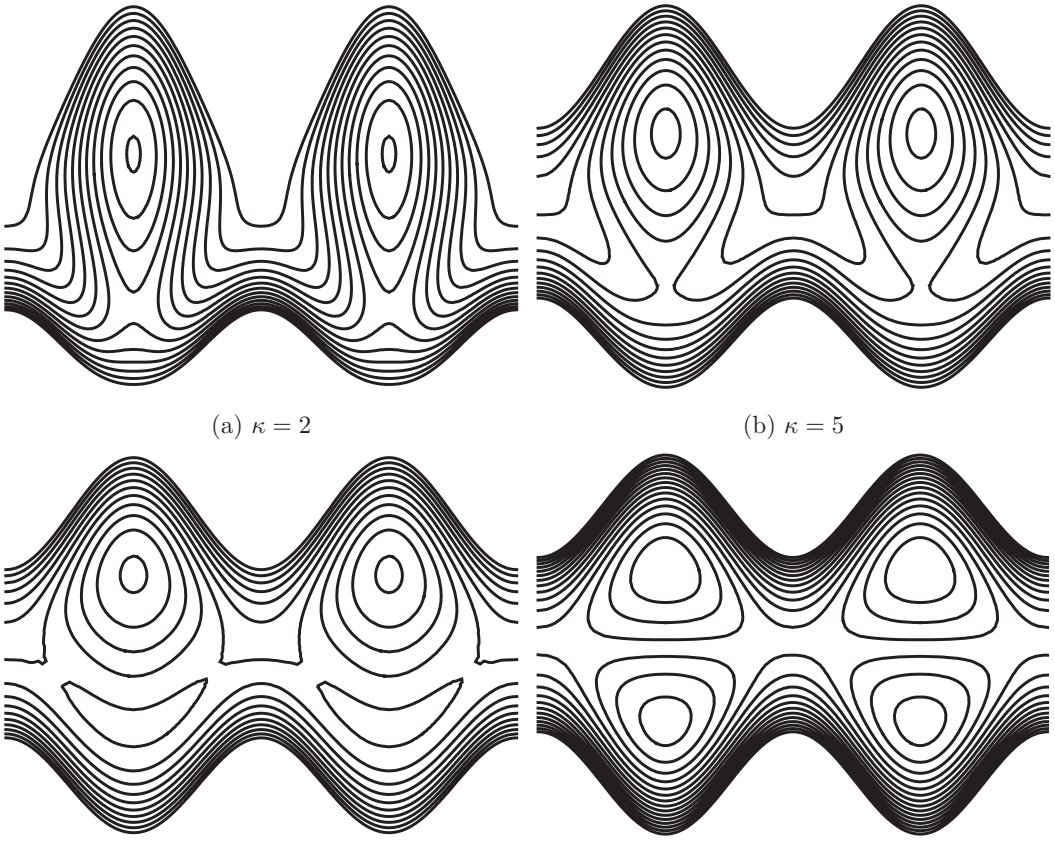

FIG. 9. Streamlines in wave frame of reference for (a) $\kappa = 2$, (b) $\kappa = 5$, (c) $\kappa = 10$, and (d) $\kappa \to \infty$.

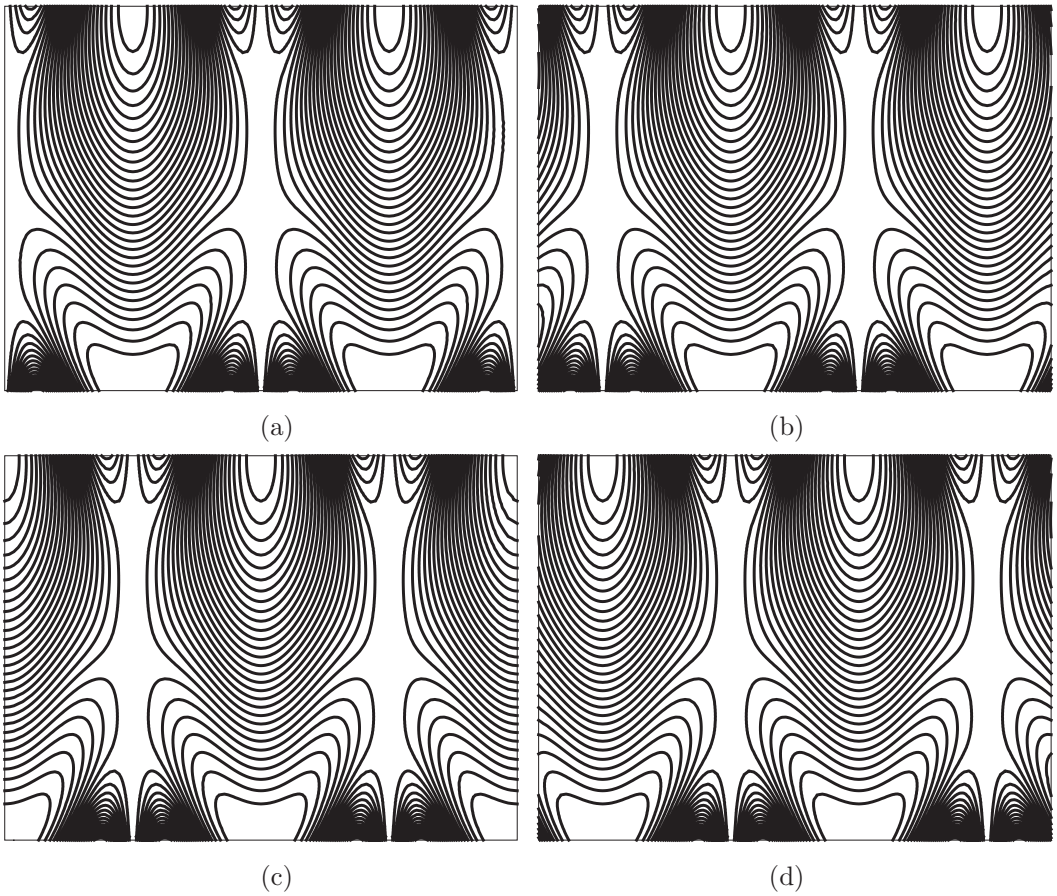

FIG. 10. Streamlines in laboratory frame of reference at five time instants for $\kappa = 2$ when $Q_T = 1.0$ and $\phi = 0.5$. (a) t = 0.0 and 1.0; (b) t = 0.25; (c) t = 0.5; (d) t = 0.75.

streamline pattern concentrated near the crest of the peristaltic waves on the walls are different in magnitudes for large values of κ, small magnitude at lower wall, and large magnitude at upper wall. However, this observation almost agrees well with the observation of Shapiro *et al.*,[2] Pozrikidis[6] for straight channel ($\kappa \to \infty$) as the bolus splits with nearly equal magnitudes and symmetrical about $r = 0$.

The effect of different curvature parameter κ values in a fixed frame of reference is illustrated with $Q_T = 1.0$ and $\phi = 0.5$ at different time points by Figures 10–12. It is observed that the streamline patterns have different amplitudes and shapes when the value of κ is small. The results of straight channel case ($\kappa \to \infty$) almost coincide with the streamline patterns shown by Pozrikidis.[6]

D. Particle trajectory and reflux phenomenon

One of the important characteristics of peristaltic flow is the reflux phenomenon. Reflux can be examined by tracking the trajectory of the massless particles in the Lagrangian frame of reference during the time the peristaltic wave completes one full cycle (Shapiro *et al.*[2]). The trajectory of a particle can be traced by integrating the simultaneous differential equations

$$\frac{dx}{dt} = u, \quad \frac{dr}{dt} = v \tag{54}$$

successively from the initial location of the particle. The integration is carried out numerically by the Runge-Kutta 4th order method. The trajectories for different channel curvatures with $\phi = 0.5$

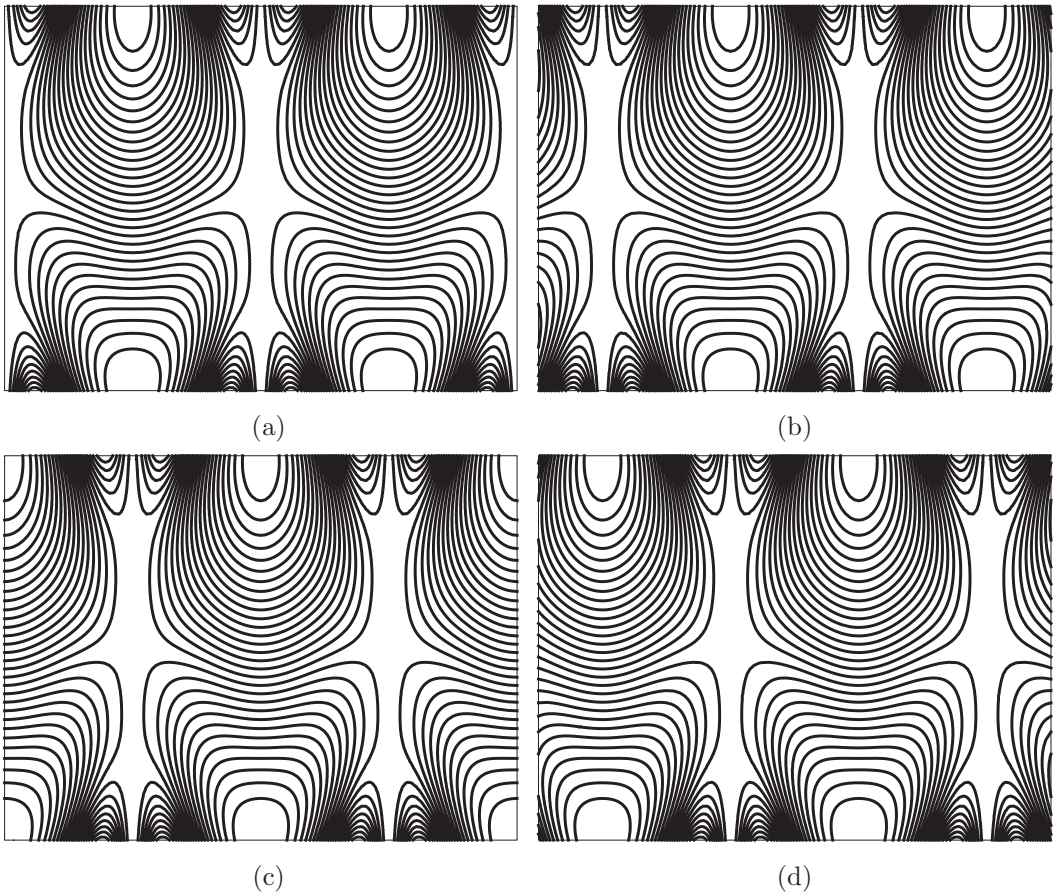

FIG. 11. Streamlines in laboratory frame of reference at five time instants for $\kappa = 5$ when $Q_T = 1.0$ and $\phi = 0.5$. (a) t = 0.0 and 1.0; (b) t = 0.25; (c) t = 0.5; (d) t = 0.75.

and $Q_T = 0.3$ are shown in Figure 13, in which the open circles indicate the initial locations and the filled circles show the locations at the end of three wave periods. Although the individual massless particles in the flow repeat the same trajectories periodically, they undergo net axial displacements, and their motion do not get closed paths. The fluid particle positioned at contraction region when time $t = 0$ experiences first a backward motion followed by a forward one, then a backward one again, as time progresses. At the end of the each particle period, the particle possesses a net positive axial displacement. The overall transport of particles near the axis possesses positive net longitudinal displacement. In our example we found that reflux occurs near upper wall, and particles will be driven in the opposite direction of the peristaltic wave, while the total net transport is in the direction of the contraction. Each fluid particle near the axis (initial location is $x = 0.71$, $r = 0.1$) experiences in three time periods a net positive displacement and its magnitude depends on channel curvature. The magnitude of these displacements decreases with an increasing channel curvature. The particle near the outer wall ($x = 0.71$, $r = 0.65$) undergoes a net negative displacement, and a net positive displacement also near the inner wall. This reflex is much in the curved channel than in the straight channel.

E. Pumping efficiency

Another important physical characteristic in pumping performance is the mechanical efficiency of pumping E. Shapiro *et al.*[2] define the mechanical efficiency of peristaltic pumping as the ratio between the average rate per wavelength at which work is done by the moving fluid against a pressure

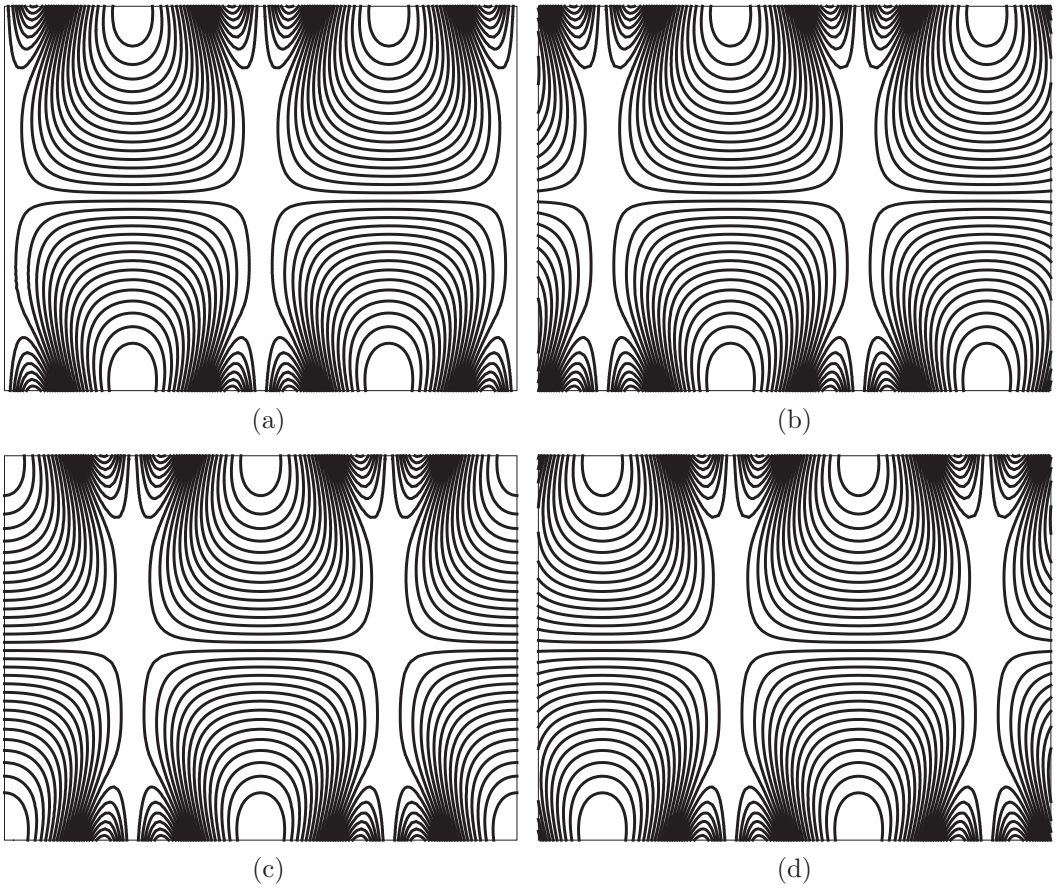

FIG. 12. Streamlines in laboratory frame of reference at five time instants for $\kappa \to \infty$ when $Q_T = 1.0$ and $\phi = 0.5$. (a) t = 0.0 and 1.0; (b) t = 0.25; (c) t = 0.5; (d) t = 0.75.

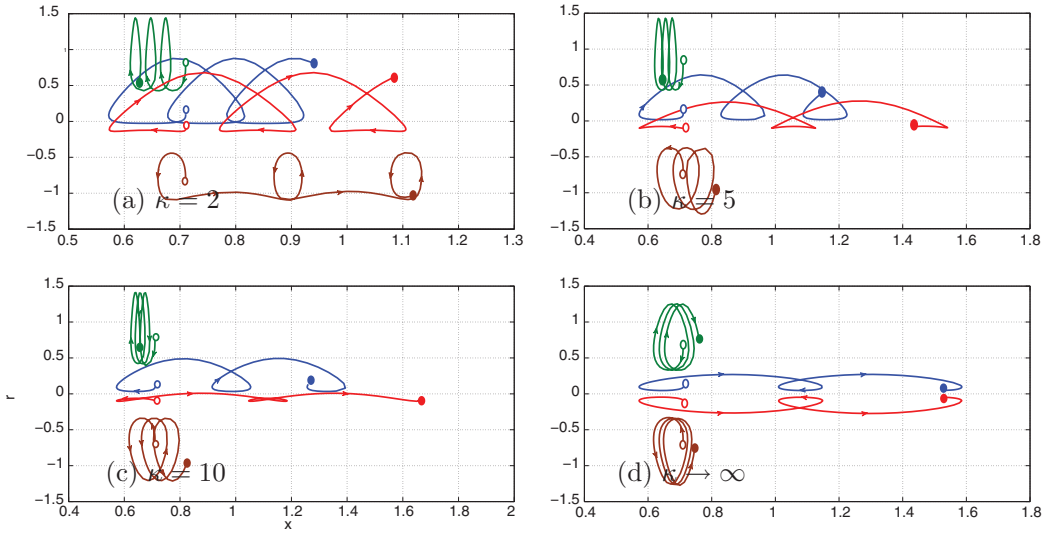

FIG. 13. Particle trajectories for (a) $\kappa = 2$, (b) $\kappa = 5$, (c) $\kappa = 10$, and (d) $\kappa \to \infty$. ○, initial locations; ●, locations at the end of three wave periods.

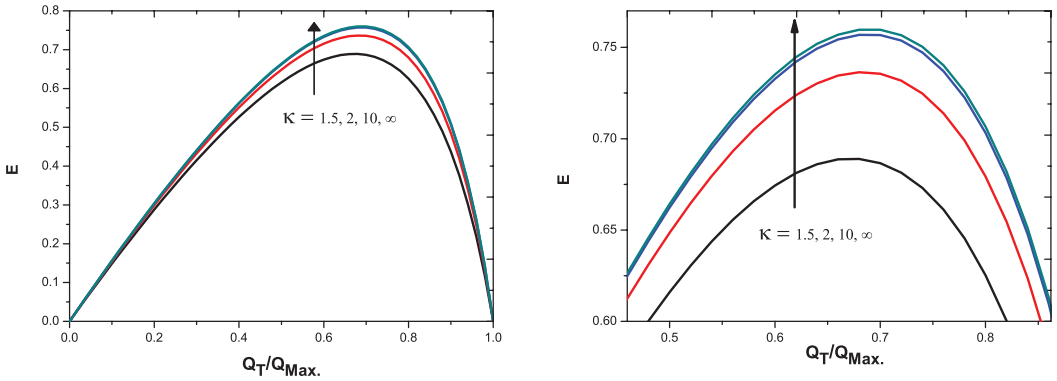

FIG. 14. (a) Mechanical efficiency against the ratio of averaged flow rate and the maximum averaged flow rate for different values of κ with $\phi = 0.6$. (b) Magnification of (a).

head and the mechanical work delivered to the wall from outside agencies:

$$E = -\frac{Q_T \Delta P_1}{\int_0^1 \int_0^1 p \frac{\partial h}{\partial t} dx dt} = -\frac{Q_T}{\phi} \frac{\Delta P_1}{\int_0^1 \frac{\partial p}{\partial X} cos(2\pi X) dX}, \tag{55}$$

where ΔP_1 is the pressure difference across one wavelength, which is given by

$$\Delta P_1 = \int_0^1 \frac{8(2 - Q_T) - 16h}{4\kappa^2 h - \frac{(\kappa^2 - h^2)^2}{h} \left(log \frac{\kappa + h}{\kappa - h}\right)^2} dX. \tag{56}$$

The numerator denotes the average rate of work done by the moving fluid over one wavelength against a pressure head and the denominator denotes the average rate of work done by the wall on the fluid over one wavelength both being averaged over one period of the wave. Moreover, the maximum flow rate is obtained by substituting $\Delta p_1 = 0$ in Eq. (56) as

$$Q_{Max.} = \frac{2 \int_0^1 \frac{1 - h}{4\kappa^2 h - \frac{(\kappa^2 - h^2)^2}{h} \left(log \frac{\kappa + h}{\kappa - h}\right)^2} dX}{\int_0^1 \frac{1}{4\kappa^2 h - \frac{(\kappa^2 - h^2)^2}{h} \left(log \frac{\kappa + h}{\kappa - h}\right)^2} dX}. \tag{57}$$

The mechanical efficiency E as a function of Q_T is plotted in Figures 14 and 15 for different values of κ and ϕ, respectively. It is observed that the pumping efficiency decreases with an increasing channel curvature. This is obvious since the pumping performance in a straight channel is comparatively higher than that in a curved channel. The mechanical efficiency increases with increasing amplitude ratio ϕ. It is physically interpreted that the pumping efficiency increases remarkably as ϕ increases due to its maximal occlusion.

F. Heat transfer analysis

In order to study the quantitative effects of temperature and heat transfer coefficient, Figures 16 and 17 are plotted. Figure 16 illustrates the effect of the temperature for several values of Brinkman number Br, pressure difference between two ends of the channel ΔP_L, curvature parameter κ, and occlusion parameter ϕ. The temperature profiles are almost parabolic. Figures 16(a) and 16(b) are plotted to see the effects of curvature parameter κ and pressure difference ΔP_L on temperature, respectively. It is observed that the temperature reduces as the curvature parameter κ and ΔP_L increase. This indicates that the temperature is a decreasing function of κ and the value of temperature reduces when pressure difference increases. It is further observed from Figures 16(c) and 16(d)

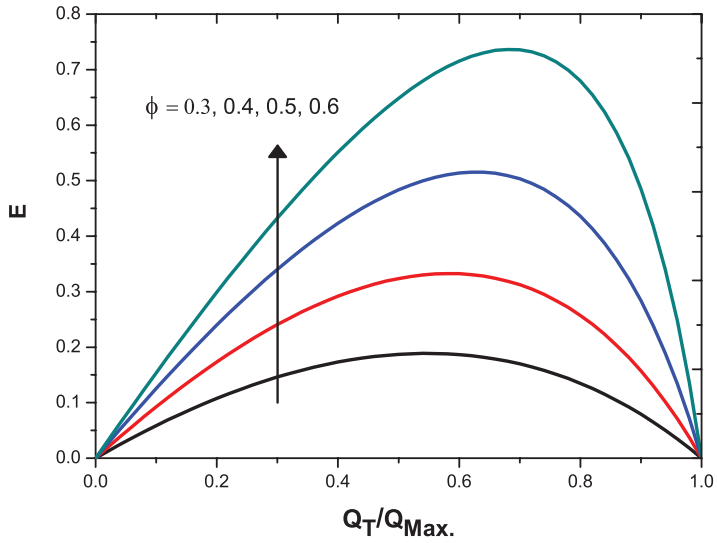

FIG. 15. Mechanical efficiency against the ratio of averaged flow rate and the maximum averaged flow rate for different values of ϕ with $\kappa = 2$.

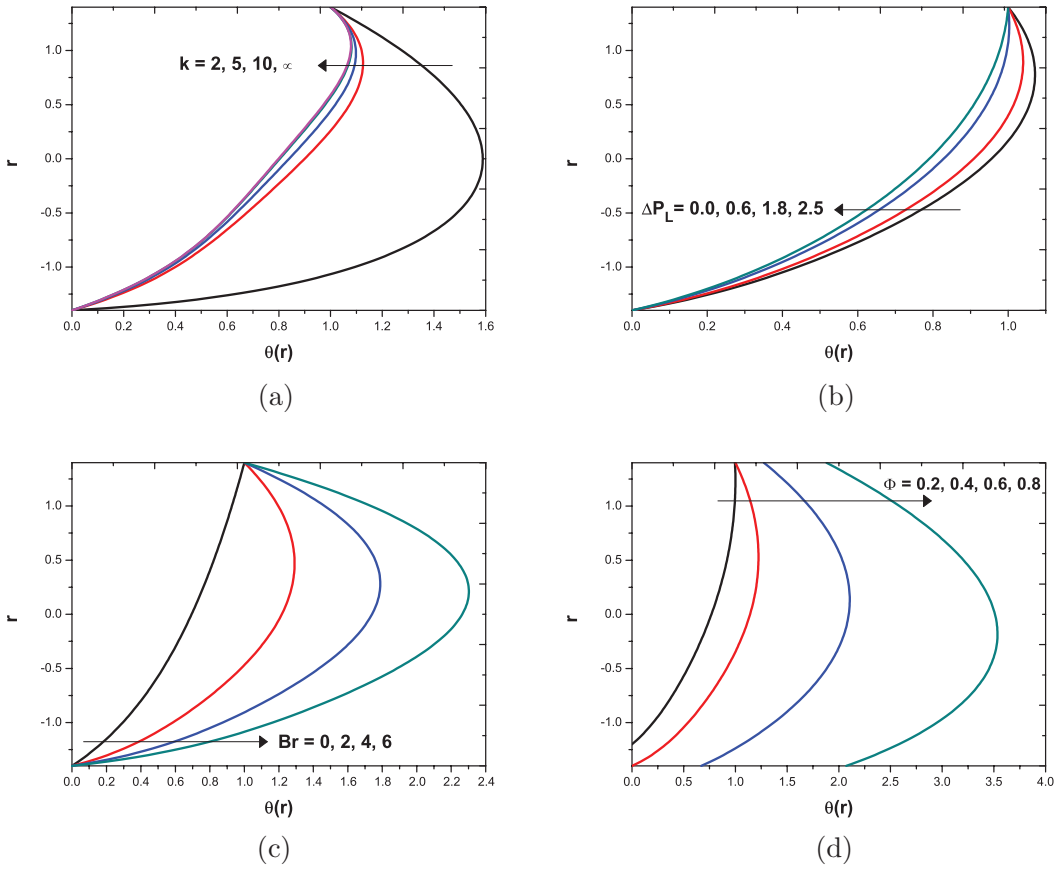

FIG. 16. Variation of temperature distribution θ for different values of curvature parameter κ, pressure difference ΔP_L, Brinkman number Br, and occlusion parameter ϕ. The other parameters chosen are (a) $\phi = 0.4$, $t = 1$, $Br = 2$, $\Delta P_L = 0$, $x = 0.5$, $L = 2$, (b) $\phi = 0.4$, $\kappa = 2$, $t = 1$, $Br = 6$, $x = 0.5$, $L = 2$, (c) $\phi = 0.4$, $\kappa = 2$, $t = 1$, $\Delta P_L = 0$, $x = 0.5$, $L = 2$, and (d) $\kappa = 2$, $t = 0$, $Br = 2$, $\Delta P_L = 0$, $x = 0.5$, $L = 2$.

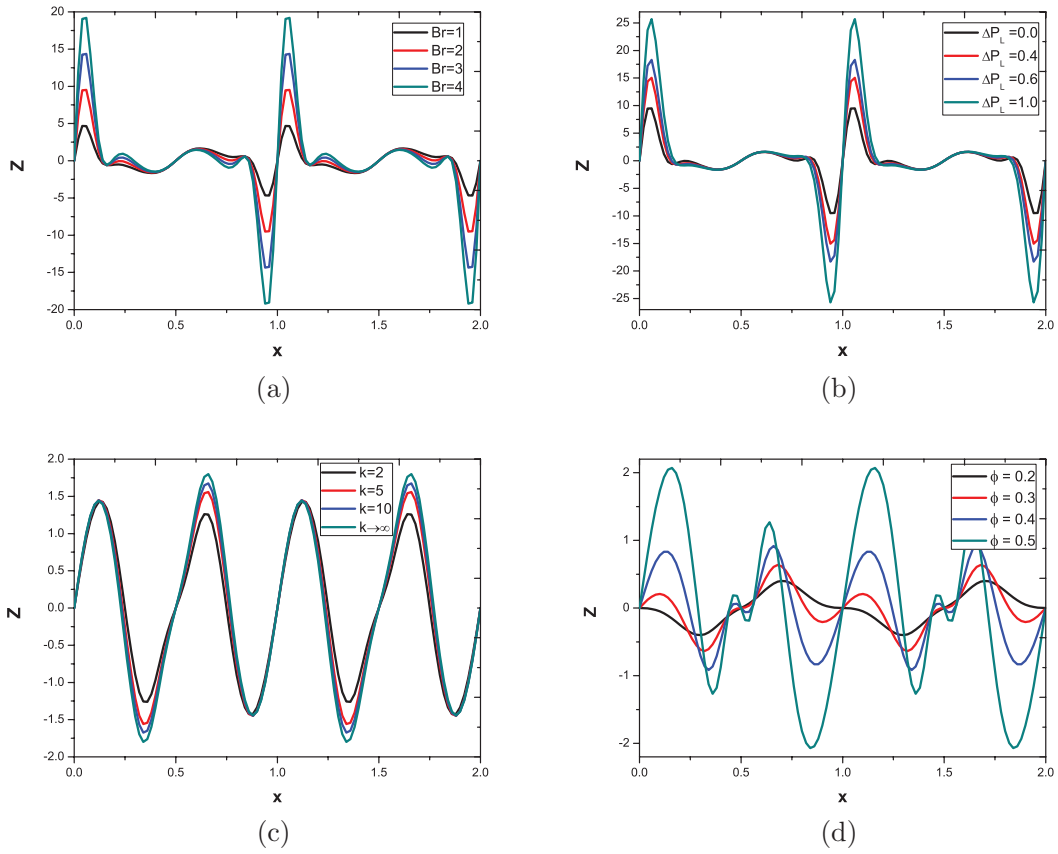

FIG. 17. Variation of Heat transfer coefficient Z at upper wall for different values of Brinkman number Br, pressure difference ΔP_L, curvature parameter κ, and occlusion parameter ϕ. The other parameters chosen are (a) $\phi = 0.6$, $\kappa = 2$, $t = 0$, $\Delta P_L = 0$, $L = 2$, (b) $\phi = 0.6$, $\kappa = 2$, $t = 0$, $Br = 2$, $L = 2$, (c) $\phi = 0.6$, $\kappa = 2$, $t = 0$, $Br = 2$, $\Delta P_L = 0$, $L = 2$, and (d) $\kappa = 2$, $t = 0$, $Br = 2$, $\Delta P_L = 0$, $L = 2$.

that the temperature increases by increasing the Brinkman number Br and occlusion parameter ϕ. Figure 17 depicts the effects of Brinkman number Br, pressure difference ΔP_L between two ends of the channel, curvature parameter κ, and occlusion parameter ϕ on the heat transfer coefficient Z at the upper wall. This figure illustrates that heat transfer coefficient is in oscillatory behavior, which may be due to peristalsis. The absolute value of peak value of heat transfer coefficient increases with increasing Br, ΔP_L, κ, and ϕ, respectively.

G. Concluding remarks

This paper presents time dependent analysis of fluid flow and heat transfer for peristaltic transport of an incompressible viscous fluid in two-dimensional curved channels. We obtained the analytical solution for fluid flow and temperature at low inertial effect when the wavelength is moderately large compared to the channel width. The features of the flow characteristics are analyzed by plotting graphs and discussed in detail. The following conclusions can be summarized:

1. The transport phenomena are mainly dependent on the curvature parameter (κ), adverse pressure gradient (ΔP_L), and the occlusion parameter (ϕ) of the curved channel.
2. The relation between pressure and flow is found to be linear, and it increases slightly with an increasing channel curvature.
3. The peristaltic flow in curved channel is low in magnitude when compared to flow in straight channel ($\kappa \to \infty$).

4. The pressure difference graphs have two different maximum or minimum values and are not cyclic for non-integral multiple of wavelength of the channel. But for integral multiple of wavelength, the maximum or minimum values of pressure difference are the same and cyclic.
5. The shear stress decreases when one moves from curved channel to straight channel.
6. The trapped bolus of fluid in wave frame contains one bolus in large curved channel. As the curvature decreases two asymmetrical boluses are formed.
7. Reflex and trapping occur well in the curved channel than in the straight channel over time averaged flow rate.
8. The effects of curvature parameter (κ) and pressure difference between channel ends (ΔP_L) on the temperature are opposite to the effect of Brinkman number (Br) and occlusion parameter (ϕ).
9. The mechanical efficiency increases with increasing curvature parameter (κ) and occlusion parameter (ϕ).
10. The temperature increases as the Brinkman number and occlusion parameter increase. It decreases as curvature parameter and pressure difference between channel ends increase.
11. The absolute value of heat transfer coefficient increases with increase in curvature parameter and all other parameters.

[1] Y. C. Fung and C. S. Yih, "Peristaltic transport," J. Appl. Mech. **35**, 669 (1968).
[2] A. H. Shapiro, M. Y. Jaffrin, and S. L. Weinberg, "Peristaltic pumping with long wavelength at low Reynolds number," J. Fluid Mech. **37**, 799 (1969).
[3] M. Y. Jaffrin and A. H. Shapiro, "Peristaltic pumping," Annu. Rev. Fluid Mech. **3**, 13 (1971).
[4] M. Y. Jaffrin, "Inertia and streamline curvature on peristaltic pumping," Int. J. Eng. Sci. **11**, 681 (1973).
[5] S. Takabatake and K. Ayukawa, "Numerical study of two dimensional peristaltic flows," J. Fluid Mech. **122**, 439 (1982).
[6] C. Pozrikidis, "A study of peristaltic flow," J. Fluid Mech. **180**, 515 (1987).
[7] M. Li and J. G. Brasseur, "Non steady peristaltic transport in finite length tubes," J. Fluid Mech. **248**, 129 (1993).
[8] G. Radhakrishnamacharya and V. Ramakrishna Murty, "Heat transfer to peristaltic transport in a non-uniform channel," Def. Sci. J. **43**, 275 (1993).
[9] B. V. Rathish Kumar and K. B. Naidu, "A numerical study of peristaltic flows," Comput. Fluids **24**, 161 (1995).
[10] E. F. Elshehawey, E. M. Elbarbary, and N. S. Elgazery, "Numerical study of a magneto-fluid motion through a porous medium between two wavyplates," Int. J. Comput. Fluid Dyn. **15**, 177 (2001).
[11] W. J. Dodds, E. T. Stewart, D. Hodges, and F. F. Zboralske, "Movement of the feline esophagus associated with respiration and peristalsis," J. Clin. Invest. **52**, 1 (1973).
[12] A. Pal and J. G. Brasseur, "The mechanical advantage of local longitudinal shortening on peristaltic transport," J. Biomech. Eng. **124**, 94 (2002).
[13] H. Sato, T. Kawai, T. Fujita, and M. Okabe, "Two dimensional peristaltic flow in curved channels," Trans. Jpn. Soc. Mech. Eng., Ser. B **66**, 679 (2000).
[14] N. Ali, M. Sajid, and T. Hayat, "Long wave length flow analysis in a curved channel," Z. Naturforsch. **65a**, 191 (2010).
[15] N. Ali, M. Sajid, T. Javed, and Z. Abbas, "Heat transfer analysis of peristaltic flow in a curved channel," Int. J. Heat Mass Transfer **53**, 3319 (2010).
[16] N. Ali, M. Sajid, Z. Abbas, and T. Javed, "Non-Newtonian fluid flow induced by peristaltic waves in a curved channel," Eur. J. Mech. B/Fluids **29**, 387 (2010).
[17] T. Hayat, M. Javed, and A. Hendi, "Peristaltic transport of viscous fluid in a curved channel with compliant walls," Int. J. Heat Mass Transfer **54**, 1615 (2011).
[18] T. Hayat, S. Noreen, and A. Alsaedi, "Effect of an induced magnetic field on peristaltic flow of non-Newtonian fluid in a curved channel," J. Mech. Med. Biol. **12**, 1250058-1–1250058-26 (2012).
[19] S. Hina, T. Hayat, M. Mustafa, O. M. Aldossary, and S. Asghar, "Effect of wall properties on the peristaltic flow of a third grade fluid in a curved channel," J. Mech. Med. Biol. **12**, 1250067-1–1250067-16 (2012).
[20] S. Hina, T. Hayat, and S. Asghar, "Heat and mass transfer effects on the peristaltic flow of Johnson-Segalman fluid in a curved channel with compliant walls," Int. J. Heat Mass Transfer **55**, 3511 (2012).
[21] S. Hina, M. Mustafa, T. Hayat, and A. Alsaedi, "Peristaltic flow of pseudo plastic fluid in a curved channel with wall properties," ASME J. Appl. Mech. **80**(2), 024501 (2013).
[22] G. A. Truskey, F. Yuan, and D. F. Katz, *Transport Phenomena in Biological Systems* (Pearson Prentice Hall, New Jersey, 2004).